



## CENTRE DE RECERCA MATEMÀTICA

This is a preprint of: *Spherically symmetric nanoparticle melting with a variable phase change temperature*

Journal Information: *CRM Preprints*,  
Author(s): F. Font, T.G. Myers.  
Volume, pages: 1-26,

DOI:[--]



CENTRE DE RECERCA MATEMÀTICA

Preprint núm. 1176

October 2013

Spherically symmetric nanoparticle  
melting with a variable phase change  
temperature

F. Font, T.G. Myers



# SPHERICALLY SYMMETRIC NANOPARTICLE MELTING WITH A VARIABLE PHASE CHANGE TEMPERATURE

F. FONT AND T. G. MYERS

**ABSTRACT.** In this paper we analyse the melting of a spherically symmetric nanoparticle, using a continuum model which is valid down to a few nanometres. Melting point depression is accounted for by a generalised Gibbs-Thomson relation. The system of governing equations involves heat equations in the liquid and solid, a Stefan condition to determine the position of the melt boundary and the Gibbs-Thomson equation. This system is simplified systematically to a pair of first-order ordinary differential equations. Comparison with the solution of the full system shows excellent agreement. The reduced system highlights the effects that dominate the melting process and specifically that rapid melting is expected in the final stages, as the radius tends to zero. The results agree qualitatively with limited available experimental data.

## 1. INTRODUCTION

Nanomaterials are currently the subject of intense investigation due to their unique properties and a wide range of novel applications such as in optical, electronic, catalytic and biomedical applications, single electron tunneling devices, nanolithography etc. [2, 17, 34, 38]. One reason for their interesting behaviour is that they have a very large ratio of surface to volume atoms which can have a significant effect on the material properties [13]. A particular example of this is the well-documented decrease in phase change temperature as the material dimensions decrease [38]. The experiments of Buffat and Borel [5] show a decrease of around 500 K for gold particles with radius slightly greater than 1 nm. The molecular dynamics simulations of Shim *et al* [38] show a 60% decrease (more than 800 K) below the bulk melt temperature for gold nanoparticles with a radius around 0.8 nm. Experiments on tin and lead have shown decreases of the order 70 K and 200 K respectively [6]. Drugs with poor water solubility may be administered as nanoparticles to improve their uptake. Bergese *et al* [4] and Liu *et al* [22] study antibiotic and antianginal drugs, which exhibit a melting point depression of around 30 K (a 10% decrease from the bulk value). Since gold has low toxicity, gold nanoparticles also make good carriers for drug and gene delivery [11, 31].

---

*Key words and phrases.* Nanoparticle melting and Mathematical model and Phase change and Gibbs-Thomson and Numerical simulation.

Given the diversity of applications of nanoparticles and that many occur at high temperatures it is important to understand their thermal response and likely phase change behaviour [38]. The present study is undertaken with this purpose in mind. In the following we will analyse the melting of a nanoparticle using continuum theory. The analysis will be based on standard phase change theory, with appropriate modification to account for the variation in the phase change temperature. We will present results primarily for the melting of gold, since much data is available for this material, however the theory is general and may be applied to other materials by using the appropriate parameter values.

Continuum theory may be applied when there is a sufficiently large sample size to ensure that statistical variation of material quantities, such as density, is small. For fluids the variation is often quoted as 1% [1]. Assuming a spherical sample Nguyen and Werely [28] suggest this level of variation requires a minimum of  $10^4$  atoms and so deduce a critical dimension of the order 10 and 90 nm for liquids and gases respectively. By comparing molecular dynamics simulations to computations based on the Navier-Stokes equations Travis *et al* [39] show that continuum theory may be applied to water flow down to around 3 nm. In the field of heat transfer and phase change it has been suggested that continuum theory requires particle radii greater than 2 nm [13] (this is based on assuming a relative temperature variation of 3%). Kofman *et al* [18] state that at scales smaller than 5 nm the melting process is discontinuous and dominated by fluctuations, Kuo *et al* [20] observed structural changes and a 'quasi-molten' state in their study of nanoparticle melting between 2-5 nm. Indeed for very small particles it may be necessary to modify the model for heat flow, one method is to augment the heat equation with an inertia term, see [40] for example. At the end of §3 we discuss the effect of this extra term on the solutions for various particle sizes. We conclude that care should be taken when modelling the phase change of very small particles and also that the continuum limit will vary depending on the material.

The standard continuum model for phase change is known as the Stefan problem. The simplest example involves solving a one-dimensional heat equation in Cartesian co-ordinates subject to constant temperature boundary conditions over a time-dependent domain whose extent is unknown '*a priori*'. At the phase change boundary,  $r = R(t)$ , the temperature is fixed at the constant bulk phase change temperature  $T(R(t), t) = T_m^*$ . The material properties remain constant throughout the process. This problem has a well-known exact solution, for more details see [3, 7, 15]. However, in reality material properties vary and there is often a jump in property values when the phase change occurs. With high curvature (such as occurs in the nano context) the phase change temperature may vary significantly: this leads to a coupling between the phase change temperature and the standard governing equations for the Stefan problem and prevents an analytical solution.

In this paper we will begin by discussing the generalised Gibbs-Thomson equation which describes the melt temperature variation. We will then describe the mathematical model appropriate for the melting of a nanosphere, subject to a fixed boundary temperature (greater than the phase change temperature). Noting that the Stefan number, the ratio of latent heat to sensible heat, is generally large for practical situations in §4 we seek approximate solutions which exploit this feature. This is first carried out for a simple one-phase reduction, where the temperature of the solid is neglected, and then for the two-phase model where both solid and liquid regions are analysed. Results are presented in §5 comparing the numerical and approximate solutions. The relation between the results and limited experimental observations is also discussed.

## 2. GENERALISED GIBBS-THOMSON RELATION

The vast majority of analyses on phase change assume that the melt temperature remains constant throughout the process. In situations where the melt temperature is variable and the density and specific heat remain approximately constant in each phase the melt temperature may be estimated from the following generalised Gibbs-Thomson relation

$$(1) \quad \left( \frac{1}{\rho_l} - \frac{1}{\rho_s} \right) (p_l - p_a) = L_m \left( \frac{T_m}{T_m^*} - 1 \right) + \Delta c \left[ T_m \ln \left( \frac{T_m}{T_m^*} \right) + T_m^* - T_m \right] + \frac{2\sigma_{sl}\kappa}{\rho_s}$$

where  $T_m$  is the temperature at which the phase change occurs,  $T_m^*$  the bulk phase change temperature,  $c$  is the specific heat,  $\Delta c = c_l - c_s$ ,  $p$  the pressure (and  $p_a$  the ambient pressure),  $\sigma$  the surface tension and  $\kappa$  the mean curvature, subscripts  $s, l$  indicate solid and liquid. A complete derivation of this equation from thermodynamical principles can be found in [3]. Various limits of equation (1) produce familiar relations. For example, with constant parameter values  $\Delta\rho = \Delta c = 0$  the standard Gibbs-Thomson equation is retrieved

$$(2) \quad T_m = T_m^* \left( 1 - \frac{2\sigma_{sl}\kappa}{\rho_s L_m} \right).$$

This demonstrates how the melt temperature decreases as the curvature at the interface increases. If  $\sigma_{sl}\kappa \ll \rho_s L_m$  then  $T_m \approx T_m^*$  is the standard constant melt temperature boundary condition.

The use of equation (2) rather than  $T_m = T_m^*$  may appear to be a rather simple modification, however it significantly complicates the system. If we consider the problem of melting a spherical particle the mean curvature will be related to the position of the phase change front  $\kappa = 1/R(t)$  and so the boundary condition  $T(R(t), t) = T_m(t)$  is time-dependent where  $T_m(t)$  must be calculated as part of the solution process. Further, the standard reduction of the two-phase to a one-phase problem ceases to make physical sense. If  $T_m = T_m^*$  is constant we may define a one-phase problem by setting the solid temperature to  $T_m^*$  for all

time. If  $T_m$  is a function of time then the one-phase problem requires the solid temperature to equilibrate instantaneously to the boundary temperature. Evans and King [9] show that the standard one-phase reduction loses energy. Myers *et al* [26] present a one-phase reduction that conserves energy and matches closely to numerical solutions of the two-phase formulation.

The relative size of the terms in (1) indicate their importance in the melting process. If the melting temperature deviates significantly from the bulk value due to curvature effects then the first term on the right hand side must have a similar magnitude to the final term. For a gold nanoparticle with radius 6 nm we find using expression (1) that  $T_m \approx T_m^* - 100$  K. Taking  $p_l - p_a = 10^5$  Pa and using the parameter values from Table 2 gives

$$(3) \quad \begin{aligned} L_m \left( \frac{T_m}{T_m^*} - 1 \right) &\sim \frac{2\sigma_{sl}\kappa}{\rho_s} = \mathcal{O}(4700) \gg \\ \Delta c \left[ T_m \ln \left( \frac{T_m}{T_m^*} \right) + T_m^* - T_m \right] &= \mathcal{O}(130) \gg \\ \left( \frac{1}{\rho_l} - \frac{1}{\rho_s} \right) (p_l - p_a) &= \mathcal{O}(0.6). \end{aligned}$$

Obviously in such a situation it is the pressure term that should be neglected first (this is achieved by setting  $\rho_l = \rho_s$  in equation (1)). Of course there are physical situations where the pressure variation is much higher and so may be the driving mechanism for the melt temperature variation, see [8], however this will not be the focus in the following work. Therefore, the version of the Gibbs-Thomson equation that will be used here is

$$(4) \quad 0 = L_m \left( \frac{T_m}{T_m^*} - 1 \right) + \Delta c \left[ T_m \ln \left( \frac{T_m}{T_m^*} \right) + T_m^* - T_m \right] + \frac{2\sigma_{sl}\kappa}{\rho_s}.$$

In Figure 1 we show a comparison of the experimentally measured melt temperature against particle radius for gold and the prediction of (4). The parameter values used in the figures are given in Table 2. The diamonds represent the experimental points, solid lines come from (4) (i.e. with  $\Delta c \neq 0$ ) and dashed lines from (2) (i.e.  $\Delta c = 0$ ). The agreement between equation (4) and experiment is excellent. The curves for  $\Delta c \neq 0$  and  $\Delta c = 0$  may appear close, but there is a significant difference in the prediction of melt temperatures. At 2 nm the two models differ by approximately 35K. In the results section we will see that this can have a large effect on the melt rate. For radii below approximately 1 nm, where  $T_m \approx 329$ K, equation (4) becomes multi-valued, this is shown in the inset. So we may assume that the generalised Gibbs-Thomson relation should not be applied below this value. Of course, since continuum theory is invalid for such small particles this does not place any extra restrictions on the mathematical model. In §5 we will cut-off solutions at  $R = 1$  nm. In fact there are a number

of different expressions for the melting point depression derived from distinct hypotheses, all of them agreeing in  $T_m - T_m^* \propto \kappa$  when the parameter values are constant [5, 18, 21, 27]. The main difference between them lies in the dependence on the interfacial energy between phases  $\sigma_{sl}$  [10, 27]. We show one example, the dash-dot curve which represents Pawlow's formula [14, eq. 1], [41] (Pawlow's formula is a form of Gibbs-Thomson relation, equation (2) where the solid-liquid surface tension  $\sigma_{sl}$  is replaced by  $\sigma_{sv} - \sigma_{lv}(\rho_s/\rho_l)^{2/3}$  and the subscript  $v$  denotes vapour). Obviously this does not accurately capture the current data set.

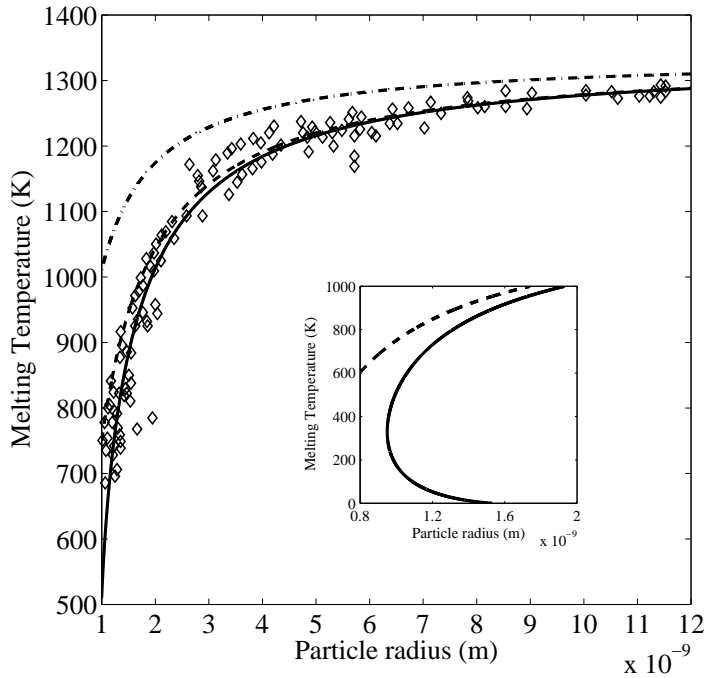


FIGURE 1. Size dependence of the melting temperature of gold nanoparticles. Solid line represents  $T_m$  from (4), dashed line corresponds to (2) and dash-dotted line to Pawlow model. Diamonds are experimental data from [5]. The subplot shows  $T_m$  from (2) and (4) for radius below 2 nm.

Nanda [27] points out that different research groups have found different dependences of  $T_m$  on the system parameters, even when examining the same material. This is attributed to different types of melting, such as liquid skin melting or homogeneous melting. Another cause for deviation at very small radius may be explained by considering the particle as a cluster of atoms. The particle is made up of bulk and surface atoms: the surface atoms are more weakly bound to the cluster than the bulk atoms and melting proceeds by the surface atoms separating from the bulk. Obviously this separation is paid for with energy (the latent



heat). With a sufficiently large cluster the energy required is relatively constant since each surface molecule is affected by the same quantity of bulk molecules. However, as the cluster decreases in size the surface molecules feel less attraction to the bulk, consequently less energy is required for separation. The change in the ratio of surface to bulk energy may also lead to a structural transition and a reduction in surface tension. Kofman et al [18] suggest that around 5 nm there is a surface induced transition in the melting process. The molecular dynamic simulations of Koga et al [19] indicate that for gold nanoparticles a structural transition occurs between 3 and 14 nm. The new particle configuration will then have a different value for the interfacial free energy. Samsonov *et al* [35] state that for metal melt nanodroplets when  $R < 4$  nm the surface tension takes the form  $\sigma_{sl} \propto R$  and their MD simulations also indicate a structural transition around this value. Sheng et al [36] specify a decrease in latent heat proportional to  $1/R$ . This leads us to the simple conclusion that the present mathematical model should not be applied down to  $R = 0$  and as already mentioned we cannot apply Gibbs-Thomson below 1 nm for gold.

Substance	$T_m^*$ (K)	$L_m$ (J/Kg)	$c_l, c_s$ (J/Kg·K)	$\rho_l, \rho_s$ (kg/m <sup>3</sup> )	$k_l, k_s$ (W/m·K)	$\sigma_{sl}$ (N/m)
Water	273	$3.34 \times 10^5$	4181/2050	$1.00 \times 10^3 / 0.92 \times 10^3$	0.55/2.20	0.03
Gold	1337	$6.37 \times 10^4$	163/129	$1.73 \times 10^4 / 1.93 \times 10^4$	106/317	0.27
Lead	600	$2.30 \times 10^4$	148/128	$1.07 \times 10^4 / 1.13 \times 10^4$	16/35	0.05

TABLE 1. Approximate thermodynamical parameter values for water, gold, and lead. The values for  $\sigma_{sl}$  are taken from [5, 18, 29].

### 3. MATHEMATICAL MODEL

The practical situation motivating the present study is the melting of nanoparticles, consequently the mathematical model is formulated as spherically symmetric. A typical configuration of the problem is illustrated in Figure 2. This depicts an initially solid, spherical nanoparticle which is heated at the surface to a temperature  $T_H > T_m^*$ . The outer region of the particle starts to melt, and the new liquid phase grows inwards until the whole solid is melted. The location of the solid-liquid interface is represented by  $R = R(t)$ . The governing equations for the two-phase problem may be written as

$$(5) \quad c_l \rho_l \frac{\partial T}{\partial t} = k_l \frac{1}{r^2} \frac{\partial}{\partial r} \left( r^2 \frac{\partial T}{\partial r} \right), \quad R < r < R_0$$

$$(6) \quad c_s \rho_s \frac{\partial \theta}{\partial t} = k_s \frac{1}{r^2} \frac{\partial}{\partial r} \left( r^2 \frac{\partial \theta}{\partial r} \right), \quad 0 < r < R$$

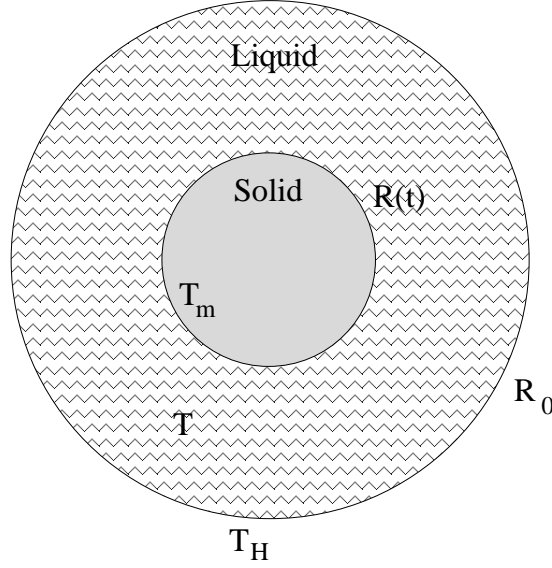


FIGURE 2. Sketch of the problem configuration.

where  $T$  represents the temperature in the liquid,  $\theta$  the temperature in the solid,  $R_0$  the initial radius of the particle and  $k$  the thermal conductivity. These equations are subject to the following boundary conditions

$$(7) \quad T(R_0, t) = T_H \quad T(R, t) = \theta(R, t) = T_m \quad \theta_r(0, t) = 0$$

and the Stefan condition

$$(8) \quad \rho_l [L_m + \Delta c(T_m - T_m^*)] \frac{dR}{dt} = k_s \frac{\partial \theta}{\partial r} \Big|_{r=R} - k_l \frac{\partial T}{\partial r} \Big|_{r=R}$$

where  $R(0) = R_0$  and  $T_m$  is specified by (4). No initial condition is imposed on the temperature in the liquid, since it does not exist at  $t = 0$ . In the solid we set  $\theta(r, 0) = T_m(0)$ , which allows us to compare the one and two phase solutions analysed in the following sections. Mathematical analyses typically invoke numerous simplifications, such as applying a single value for the thermal properties irrespective of phase or a constant phase change temperature. In the following we will only impose constant density (in line with neglecting pressure variation in the Gibbs-Thomson relation). This significantly simplifies the analysis and it is the material property which has the least variation (from Table 2 we see that  $\rho$  increases by approximately 10% when ice melts whilst  $c$  doubles and  $k$  decreases by a factor 4).

Introducing the dimensionless variables

$$(9) \quad \hat{T} = \frac{T - T_m^*}{T_H - T_m^*} \quad \hat{\theta} = \frac{\theta - T_m^*}{T_H - T_m^*} \quad \hat{r} = \frac{r}{R_0} \quad \hat{R} = \frac{R}{R_0} \quad \hat{t} = \frac{k_l}{\rho_l c_l R_0^2} t$$

in (5)–(8) and dropping the hats the following nondimensional formulation is obtained

$$(10) \quad \frac{\partial T}{\partial t} = \frac{1}{r^2} \frac{\partial}{\partial r} \left( r^2 \frac{\partial T}{\partial r} \right), \quad R < r < 1$$

$$(11) \quad \frac{\partial \theta}{\partial t} = \frac{k}{c} \frac{1}{r^2} \frac{\partial}{\partial r} \left( r^2 \frac{\partial \theta}{\partial r} \right), \quad 0 < r < R$$

with boundary conditions  $T(1, t) = 1$ ,  $T(R, t) = \theta(R, t) = T_m(t)$ ,  $\theta_r(0, t) = 0$  and the Stefan condition

$$(12) \quad [\beta + (1 - c)T_m] \frac{dR}{dt} = k \frac{\partial \theta}{\partial r} - \frac{\partial T}{\partial r} \Big|_{r=R}.$$

The nondimensional melting temperature  $T_m$  is scaling in the same manner as  $T$  and determined from

$$(13) \quad 0 = \beta \left( T_m + \frac{\Gamma}{R} \right) + \frac{(1 - c)}{\delta T} \left[ \left( T_m + \frac{1}{\delta T} \right) \ln (T_m \delta T + 1) - T_m \right].$$

The dimensionless parameters are defined by

$$c = c_s/c_l \quad k = k_s/k_l \quad \beta = L_m/c_l \Delta T$$

$$\delta T = \Delta T/T_m^* \quad \Gamma = 2\sigma_{sl}T_m^*/R_0\rho_l L_m \Delta T$$

where  $\Delta T = T_H - T_m^*$ .

McCue et al [24] carry out a mathematical analysis of a similar system using the standard Gibbs-Thomson relation, equation (2). Their expression for interfacial energy makes this equivalent to Pawlow's formula. This choice corresponds to setting  $c = 1$  in equation (13) and changing the value of  $\Gamma$ . In the Stefan condition they apply  $c \neq 1$ . They go on to analyse small time and large Stefan number solutions and discuss the system behaviour as  $R \rightarrow 0$ . In the following we will focus more on the physical problem, which requires large Stefan number. Accepting that continuum theory does not hold as  $R \rightarrow 0$  we do not analyse that limit. We retain all terms in equation (13) and show that setting  $c = 1$  is only valid for large particles. In [43] the one-phase limit with  $c = 1$  is analysed for inward solidification, so the phase change temperature increases as the solidification front moves inwards.

Note, as the particle size decreases the heat equations may require some adjustment. One such method is to include an additional inertia term  $\tau_v/\tau T_{tt}$ , see [40] for example, where  $\tau_v$  is a relaxation time (of the order 1ps) and  $\tau = \rho_l c_l L^2/k_l$  is the diffusive time-scale. For a 100 nm gold nanoparticle, neglecting this term will lead to errors of the order 0.3% however, due to the  $L^2$  term, with a 10 nm particle the error may be as much as 30%. Consequently, as pointed out in the introduction the present theory will lose accuracy as the particle size decreases.

## 4. SOLUTION METHOD

To clarify the analytical methods used in the following section, we will begin by analysing the one-phase problem. There is a long history of studies of one-phase solidification typically neglecting melting point depression, see [23, 32] for example. This approximation involves setting the solid to the melt temperature  $\theta = T_m(t)$ . It may also be viewed as a large  $k/c$  approximation (for gold  $k/c \approx 3.8$ ). Evans and King [9] point out that in this limit a thermal boundary layer will exist and the one-phase formulation loses energy. However, their proposed solution to the problem is not valid for physically realistic systems and, whilst conserving energy, is less accurate than the standard reduction. An accurate one-phase formulation which conserves energy is derived in [26], this adds an acceleration term  $R_{tt}$  to the Stefan condition. However, in §4.1 we will use the standard reduction since it is simple to formulate and leads to relatively small errors (when compared to those introduced by using continuum theory on very small particles). In §4.2 we extend the one-phase solution to the more physically realistic two-phase case and in §5 we show that the one-phase approximation of §4.1 is accurate for large particles.

**4.1. One-phase reduction.** Assuming  $k/c \gg 1$  in (11) at leading order we may neglect the  $\theta_t$  term and find  $\theta = T_m(t)$  is the solution satisfying the reduced equation and boundary conditions. This permits us to eliminate the term  $k\theta_r$  from (12) and the problem reduces to

$$(14) \quad \frac{\partial T}{\partial t} = \frac{1}{r^2} \frac{\partial}{\partial r} \left( r^2 \frac{\partial T}{\partial r} \right), \quad T(1, t) = 1, \quad T(R, t) = T_m$$

where  $T$  is the temperature of the liquid phase,  $T_H$  is the temperature at the surface of the particle and  $T_m$  is the melting temperature specified by (13), with the Stefan condition

$$(15) \quad [\beta + (1 - c)T_m] \frac{dR}{dt} = - \left. \frac{\partial T}{\partial r} \right|_{r=R}.$$

The system requires no initial condition on the temperature, since at  $t = 0$  there is no liquid, however we must then apply a condition on the domain,  $R(0) = 1$ . The Stefan number,  $\beta = L_m/c_l \Delta T$ , is a characteristic nondimensional parameter of our system that provides a measure of the importance of the latent heat released in the phase change,  $L_m$ , relative to the heat required to increase the temperature of the material by  $\Delta T$  (that is  $c_l \Delta T$ ). For example, for a temperature increase of  $\Delta T = 10$  K we have  $\beta \approx 8, 40, 12$  for water, gold and lead, respectively. Obviously, the smaller the increase  $\Delta T$  the larger the value of  $\beta$ . Due to the small volume of the nanoparticles the energy required to melt them is also small: any increase above the melting temperature,  $\Delta T$ , on the nanoparticle surface is enough to almost instantaneously melt it. Hence, working in a large Stefan number regime, where  $\beta \gg 1$ , is a sensible assumption.

The standard large  $\beta$  reduction of the Stefan problem involves re-scaling time,  $t = \beta\tau$ , so that equations (14)–(15) become

$$(16) \quad \frac{1}{\beta} \frac{\partial T}{\partial \tau} = \frac{1}{r^2} \frac{\partial}{\partial r} \left( r^2 \frac{\partial T}{\partial r} \right), \quad T(1, \tau) = 1, \quad T(R, \tau) = T_m,$$

$$(17) \quad \left[ 1 + \frac{(1-c)}{\beta} T_m \right] \frac{dR}{d\tau} = - \frac{\partial T}{\partial r} \Big|_{r=R}.$$

Assuming  $1/\beta \ll 1$ , it may be used as the small parameter for a perturbation solution of the form  $T = T_0 + T_1/\beta + \mathcal{O}(1/\beta^2)$  [16]. Substituting this series into (16) and equating like powers of  $1/\beta$  yields a sequence of differential equations. If the sequence is cut at the first order, we obtain

$$(18) \quad \mathcal{O}(1): \quad 0 = \frac{1}{r^2} \frac{\partial}{\partial r} \left( r^2 \frac{\partial T_0}{\partial r} \right), \quad T_0(1, \tau) = 1, \quad T_0(R, \tau) = T_m$$

$$(19) \quad \mathcal{O}(1/\beta): \quad \frac{\partial T_0}{\partial \tau} = \frac{1}{r^2} \frac{\partial}{\partial r} \left( r^2 \frac{\partial T_1}{\partial r} \right), \quad T_1(1, \tau) = 0, \quad T_1(R, \tau) = 0$$

with respective solutions

$$(20) \quad T_0 = 1 + (T_m - 1) \frac{R}{r} \left( \frac{1-r}{1-R} \right)$$

$$(21) \quad T_1 = \frac{(3R\mu_1 + T_m - 1)}{6(1-R)^2} \left\{ \left[ (3-r)r - \frac{2}{r} \right] - \frac{R}{r} \left( \frac{1-r}{1-R} \right) \left[ (3-R)R - \frac{2}{R} \right] \right\} \frac{dR}{d\tau}$$

where

$$(22) \quad \mu_1 = \frac{\Gamma(1-R)}{3R^2 \left[ 1 + \frac{(1-c)}{\beta \delta T} \ln(T_m \delta T + 1) \right]}.$$

At this point, we already have an approximate solution for the temperature,  $T \approx T_0 + T_1/\beta$ . However, this solution contains the variables  $R$  and  $T_m$  which are still unknown. We obtain an equation for  $R(\tau)$  by substituting for  $T$  in the Stefan condition (17)

$$(23) \quad \frac{dR}{d\tau} = \frac{(T_m - 1)}{R(1-R)} \left[ 1 + \frac{1}{\beta} \left\{ \left( 1 - c - \frac{1}{3R} \right) T_m + \frac{1}{3R} - \mu_1 \right\} \right]^{-1}.$$

We obtain an equation for  $T_m$  by taking the time derivative of (13). This is,

$$(24) \quad \frac{dT_m}{d\tau} = \frac{3\mu_1}{1-R} \frac{dR}{d\tau}.$$

The equations (23) and (24) form a pair of coupled ordinary differential equations.

This is a much simpler system to solve than the initial partial and ordinary differential equation system which applied over an unknown domain. Note that the initial condition for  $R$  is  $R(0) = 1$  and the initial condition for  $T_m$  is obtained by substituting  $R = 1$  in (13) and solving the subsequent nonlinear equation. We could make some analytical progress on the solution for  $R$  by using an expansion of the form  $R \approx R_0 + R_1/\beta$  on equation (23), but this turns out to be rather complex whilst using any standard numerical tool, such as Matlab routine `ode15s`, on (23)–(24) is straightforward.

Equations (23, 24) have two obvious singularities at  $R = 0, 1$ , where the velocity  $R_\tau = \infty$ . The initial singularity, when  $R = 1$ , is unphysical and a result of the boundary condition. The Stefan condition states that the velocity  $R_\tau$  is proportional to the temperature gradient  $T_r$ . The temperature gradient  $T_r \approx (T_m(t) - T(1, t))/(1 - R)$  and since  $T_m(0) \neq T(1, 0)$  it will be infinite at  $\tau = t = 0$ , when  $R = 1$ . This singularity is typical for Stefan problems where the boundary temperature is fixed and could be avoided by applying a different condition, such as a heat flux or kinetic undercooling [9]. The second singularity, at  $R = 0$  is a result of the physical system and not related to the initial or boundary conditions. The existence of a single singularity in the system may be inferred from Figure 1, the gradient  $T_m \rightarrow -\infty$  as  $R \rightarrow 0$  (but nowhere else). Note, this singularity could cause a problem with our perturbation solution, which requires the  $\mathcal{O}(1/\beta)$  term to be much smaller than the leading order, hence our solution may break down as  $R \rightarrow 0$ . However, we have also made it clear that our solution must break down due to the failure of the Gibbs-Thomson relation and continuum theory in this limit so this issue is not a great mathematical concern.

The governing equations contain various parameters which control the behaviour to differing extents: the largest effect will be due to leading order terms. Equation (24) is simply the derivative of the Gibbs-Thomson relation (13) which, after neglecting  $\mathcal{O}(1/\beta)$  terms, shows that  $T_m \approx -\Gamma/R$ . The leading order of equation (23) shows the  $R$  variation is proportional to  $T_m - 1 = -1 - \Gamma/R$ . The rate of decrease of the solid radius is therefore controlled primarily by  $\Gamma = 2\sigma_{sl}T_m^*/(R_0\rho_l L_m \Delta T)$ , that is, a particle will melt rapidly if it has high surface tension or bulk melt temperature or low density and latent heat. For any given material these parameters are fixed so the actual melting can only be controlled by the initial particle radius  $R_0$  and the temperature change  $\Delta T$ .

The one phase model is sometimes reduced by making assumptions on the parameter values. A common reduction involves equating the specific heats in each phase,  $c_l = c_s$  (or  $c = 1$  in our nondimensional notation) [43]. This assumption is convenient because it removes  $T_m$  from the Stefan condition (15) and reduces the generalized Gibbs-Thomson equation (13) to the standard, simpler version where  $T_m \propto 1/R$ . Wu *et al* [42] take  $c = 1$  in the Gibbs-Thomson relation but  $c \neq 1$  in the Stefan condition. In our case, setting  $c = 1$  leads to  $T_m = -\Gamma/R$  and equation (23) becomes

$$(25) \quad \frac{dR}{dt} = -\frac{R + \Gamma}{\beta R^2(1 - R)} \left[ \beta + \frac{(1 + \Gamma)}{3R} \right]^{-1}.$$

This may be integrated to

$$(26) \quad -\beta(1 - R^3) + a(1 - R^2) - b(1 - R) + b\Gamma \ln \left( \frac{\Gamma + 1}{\Gamma + R} \right) = 3t$$

where  $a = (\Gamma + 1)(3\beta - 1)/2$  and  $b = \Gamma^2(3\beta - 1) + \Gamma(3\beta - 2) - 1$ . In the results section we will show calculations with  $R_0 = 10, 100$  nm, which changes the value of  $\Gamma$ , for sufficiently large  $R_0$  the curves with  $c \neq 1$ ,  $c = 1$  coincide.

A further reduction can be made by removing the Gibbs-Thomson effect from the model. In other words, considering a constant melt temperature  $T_m = 0$ , this is equivalent to setting  $\Gamma = 0$  in (26). Then,

$$(27) \quad -\beta(1 - R^3) + \frac{(3\beta - 1)}{2}(1 - R^2) - R + 1 = 3t.$$

This will also be examined in the results section.

In summary, we provide three different solution forms to the one-phase model (14)–(15). The solutions correspond to three levels of approximation: (i) The first and most general one is obtained by integrating (23)–(24) numerically, this takes into account the difference between the specific heats ( $c \neq 1$ ) in the Stefan condition and the full expression for the Gibbs-Thomson equation; (ii) the second solution comes from (26) where we take  $c = 1$ ,  $\Gamma \neq 0$ ; (iii) the third is (27) where we have assumed  $c = 1$  and  $\Gamma = 0$ . This last one, in fact, corresponds to the solution of the classical one-phase Stefan problem in the sphere, analysed by previous authors [3, 15].

**4.2. Two-phase formulation.** In the previous section we presented the one-phase solution that neglects the solid temperature. We now build on this solution to model the two-phase process specified by equations (10)–(13).

The same rescaling of the time variable,  $t = \beta\tau$ , can be applied to the equation for the temperature in the solid, equation (11), and  $\theta$  expanded in terms of  $1/\beta$ . This, leads to

$$(28) \quad \mathcal{O}(1) : \quad 0 = \frac{1}{r^2} \frac{\partial}{\partial r} \left( r^2 \frac{\partial \theta_0}{\partial r} \right), \quad \frac{\partial \theta_0}{\partial r} \Big|_{r=0} = 0, \quad \theta_0(R, \tau) = T_m$$

$$(29) \quad \mathcal{O}(1/\beta) : \quad \frac{\partial \theta_0}{\partial \tau} = \frac{k}{c} \frac{1}{r^2} \frac{\partial}{\partial r} \left( r^2 \frac{\partial \theta_1}{\partial r} \right), \quad \frac{\partial \theta_1}{\partial r} \Big|_{r=0} = 0, \quad \theta_1(R, \tau) = 0$$

with solution

$$(30) \quad \theta_0 = T_m, \quad \theta_1 = -\frac{\mu_2}{2kR}(R^2 - r^2) \frac{dR}{d\tau}$$

where

$$(31) \quad \mu_2 = \frac{c}{3R} \frac{\Gamma}{\left[1 + \frac{(1-c)}{\beta\delta T} \ln(T_m\delta T + 1)\right]}.$$

Note, since the leading order heat equation for  $\theta_0$  does not have a time derivative no initial condition is required. However, the one-phase reduction involves the assumption  $\theta(r, t) = T_m(t)$ , so if we wish to compare with the one-phase problem we require  $\theta(r, 0) = T_m(0)$  and indeed this is consistent with the boundary conditions given in (28).

The Stefan condition now leads to

$$(32) \quad \frac{dR}{d\tau} = \frac{(T_m - 1)}{R(1 - R)} \left[ 1 + \frac{1}{\beta} \left\{ \left( 1 - c - \frac{2}{R} \right) T_m + \frac{2}{R} - \mu_1 - \mu_2 \right\} \right]^{-1}.$$

The introduction of the solid temperature has modified equation (23) at first order by the term  $\mu_2$ , which comes from the  $\theta_1$  expression. Since  $\mu_2 > 0$  this term acts to speed up the melting process. In the following section we will see that the temperature in the solid does indeed contribute towards faster melting.

## 5. RESULTS AND DISCUSSION

We now present a set of results corresponding to the solutions found in the previous section. First, we show the different solutions obtained for the one-phase model and compare them with numerical solutions using a method similar to that described in [25]. This is a semi-implicit finite difference scheme that discretizes implicitly for the temperature and explicitly for the moving front. The heat equation is converted into a planar equation with the transformation  $T = u/r$  and the moving boundary is immobilized by means of the change of variable  $\xi = (r - R)/(1 - R)$ , to fix the domain. Second, we show the solution of the full two-phase model and compare it with that for the one-phase problem. Finally, we use the one and two-phase models to calculate the melting times for different initial particle sizes and external temperatures. We also show the temperature distribution in both phases as the melting proceeds.

The plots in Figure 3 show the position of the solid-liquid interface as a function of time for the one-phase problem with an initial dimensional radius  $R_0 = 10$  nm and two different values of the Stefan number  $\beta = 100$  and  $\beta = 10$ . The dimensional values may be retrieved by multiplying  $R$  by  $R_0$  and  $t$  by the time-scale  $\rho_l c_l R_0^2 / k_l \approx 2.66 \times 10^{-12}$  s. The solid and dashed lines represent the perturbation and numerical results respectively. Curve (i) corresponds to the solution of (23)–(24), curve (ii) corresponds to the solution of (26) resulting from setting  $c_l = c_s$  (hence  $c = 1$ ) and curve (iii) is the solution (27) obtained by setting  $c = 1$ ,  $\Gamma = 0$  (hence  $T_m(t)$  is constant). As discussed earlier, the plots are cut-off at  $R = 0.1$  which corresponds to a dimensional value  $0.1R_0$ , where  $R_0 = 10$  nm. Beyond this both the numerical and perturbation solutions of equations (23)–(24) break down due to the failure of the Gibbs-Thomson relation (as seen on the inset in Figure 1



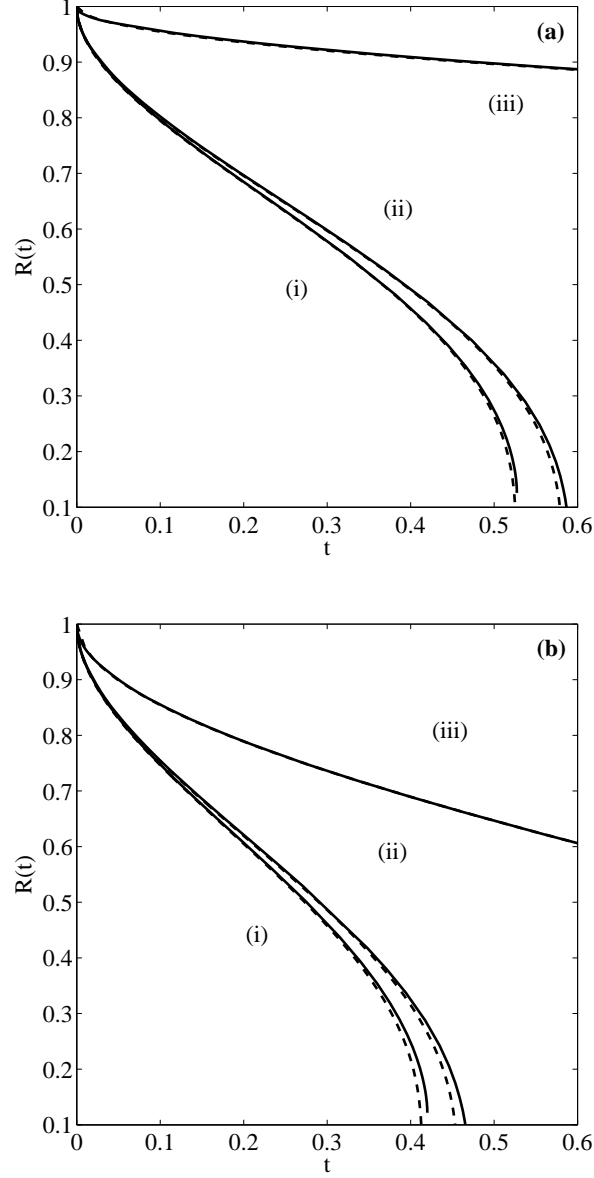


FIGURE 3. Position of the non-dimensional melting front  $R(t)$  for a nanoparticle with initial dimensional radius  $R_0 = 10$  nm, (a):  $\beta = 100$  (b)  $\beta = 10$ . Curve (i) is the solution of (23)–(24), (ii) the solution of (26) and (iii) the solution of (27).

there is no real value of  $T_m$  for  $R < 1$  nm). For large Stefan number it is clear that the asymptotics and numerics agree very well, with only a slight difference showing as  $R \rightarrow 0$ . Curves (i) and (ii) exhibit high velocities  $R_t \rightarrow \infty$  both

initially and as  $R \rightarrow 0$ . This behaviour is obvious from the factor  $1/(R(1-R))$  in equation (23). The rapid melting as  $R \rightarrow 0$  has been predicted experimentally and depicted schematically in [18, Fig.1b] and also noted in [24]. Curve (ii), with  $c = 1$ , shows a melt time approximately 11% slower than that of curve (i). This is significantly greater than the error introduced by the perturbation (since we neglect terms of  $\mathcal{O}(1/\beta^2)$  and  $\beta = 100$ , the perturbation errors are of  $\mathcal{O}(10^{-2}\%)$ ).

In Figure 4 we show the evolution of  $R(t)$  for a nanoparticle with an initial radius of  $R_0 = 100$  nm for  $\beta = 100$  and  $\beta = 10$ , the time-scale  $\rho_l c_l R_0^2 / k_l \approx 2.66 \times 10^{-10}$ . In this case, the solution breaks down when  $R \approx 1$  nm/100 nm = 0.01. In contrast to the previous figure we observe that the solutions (i) and (ii) are almost identical for most of the process, indicating the change in specific heat is not important (at least for the melting of gold) for sufficiently large particles. The difference between Figures 3 and 4 is the value of  $R_0$  which changes from 10 to 100 nm. Earlier we pointed out that  $\Gamma$  is the main controlling parameter where  $\Gamma \propto 1/R_0$ . From the figures we can see that a large change in  $\Gamma$  does indeed result in a large change in melting times.

TABLE 2. Melting times computed with the one-phase model.

	Melting times (s)		
	$R_0 = 10$ nm	$R_0 = 100$ nm	$R_0 = 500$ nm
$\beta = 100$ ( $T_H \approx 1341$ K)	$1.56 \cdot 10^{-12}$	$1.20 \cdot 10^{-9}$	$7.35 \cdot 10^{-8}$
$\beta = 10$ ( $T_H \approx 1376$ K)	$1.25 \cdot 10^{-12}$	$0.39 \cdot 10^{-9}$	$1.25 \cdot 10^{-8}$
$\beta = 5$ ( $T_H \approx 1415$ K)	$1.05 \cdot 10^{-12}$	$0.24 \cdot 10^{-9}$	$0.71 \cdot 10^{-8}$

TABLE 3. Melting times computed with the two-phase model.

	Melting times (s)		
	$R_0 = 10$ nm	$R_0 = 100$ nm	$R_0 = 500$ nm
$\beta = 100$ ( $T_H \approx 1341$ K)	$1.44 \cdot 10^{-12}$	$1.19 \cdot 10^{-9}$	$7.33 \cdot 10^{-8}$
$\beta = 10$ ( $T_H \approx 1376$ K)	$1.15 \cdot 10^{-12}$	$0.39 \cdot 10^{-9}$	$1.25 \cdot 10^{-8}$
$\beta = 5$ ( $T_H \approx 1415$ K)	$0.97 \cdot 10^{-12}$	$0.24 \cdot 10^{-9}$	$0.70 \cdot 10^{-8}$

Figure 5 displays a comparison of the one and two-phase formulations when  $\beta = 100$ . The difference between the formulations lies in the  $\mu_2$  term of the Stefan condition (32). Since  $\mu_2 \propto \Gamma \propto 1/R_0$  we expect the greatest variation for

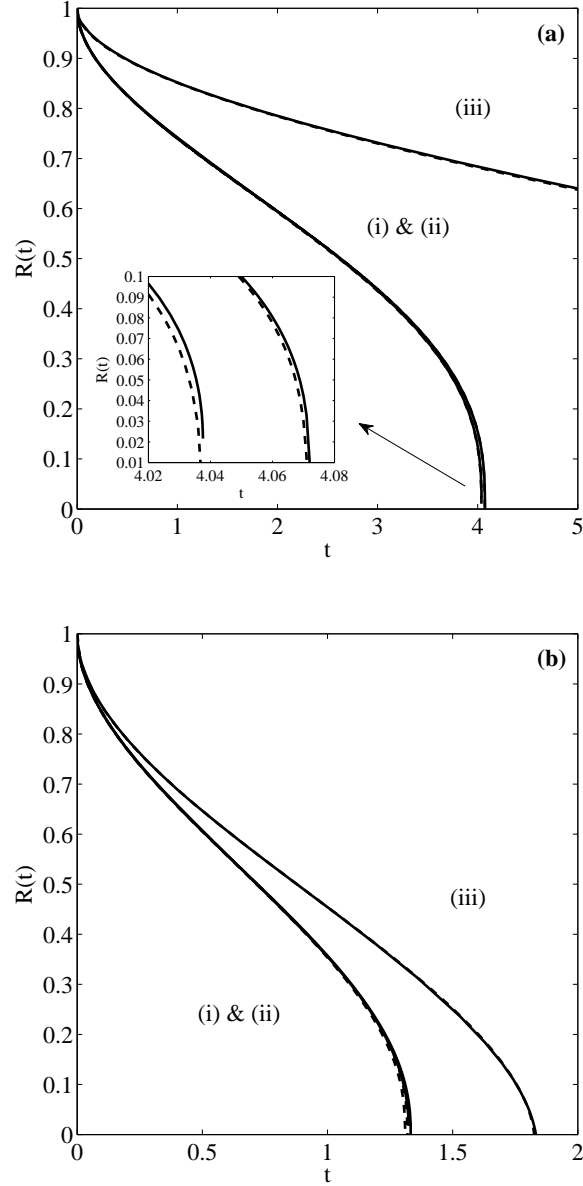


FIGURE 4. Position of the non-dimensional melting front  $R(t)$  for a nanoparticle with initial radius  $R_0 = 100$  nm, (a):  $\beta = 100$  (b)  $\beta = 10$ . Curve (i) is the solution of (23)–(24), (ii) the solution of (26) and (iii) the solution of (27).

small values of  $R_0$ . Figure 5a shows a comparison of results for  $R_0 = 10$  nm and it is clear that there is a significant difference in the curves. However, in Figure 5b, where  $R_0 = 100$  nm the curves are virtually identical (the blow-up shows the

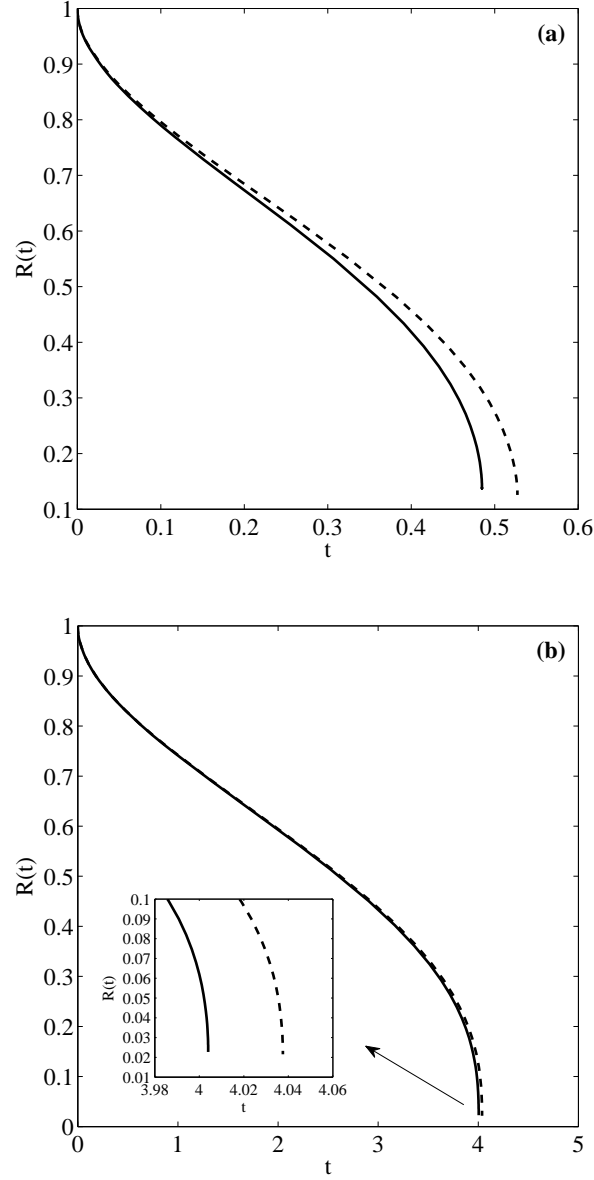


FIGURE 5. Comparison between one and two-phase solutions for  $\beta = 100$ , (a)  $R_0 = 10$  nm (b)  $R_0 = 100$  nm.

small percentage difference for small  $R$ ). Consequently we may conclude that for a given material the variation in specific heat and the use of one or two phase formulations is only important for very small nanoparticles (large values of  $\Gamma$ ). This conclusion on the one and two-phase formulation may be verified through Tables 2 and 3, which show melting times for multiple particle sizes and Stefan

numbers. In all cases the melting times are relatively close, with the largest differences occurring with the smallest particles.

The results agree well with limited available experimental data. Our calculations show that when  $R_0 = 10$  nm the melting time lies in the picosecond range, with  $R_0 = 100$  nm the melting times go from a few to several hundred picoseconds, with  $R_0 = 500$  nm melting times are well above the nanosecond scale. Pech *et al* [30] track the melting process of gold nanoparticles when they are heated by a laser beam with power 30 mW. They find that the melting process is faster than 100 ps for particles with  $R_0 = 50$  nm. By assuming the same power and a regular spot laser beam of 4  $\mu$ m diameter we obtain a power per unit area of  $2.39 \times 10^5$  W/cm<sup>2</sup>. Using this value in [12, Fig.1] the temperature increase at the nanoparticle surface is about  $\Delta T \approx 40$  K. In our model, this temperature increase corresponds to  $\beta = 10$  and our predicted time to complete melting for a particle of this size is 73.3 ps. In [33] experimental observation of nanoparticle melting is carried out for particles with  $R_0 = 2$  and 20 nm with melting times in the picosecond range.

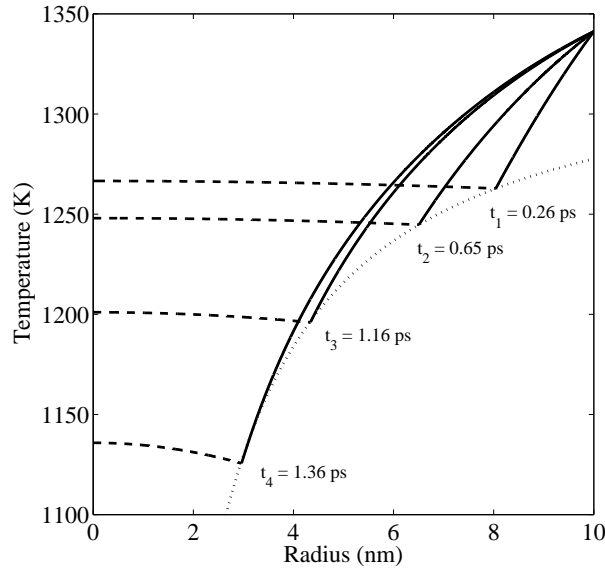


FIGURE 6. Blue is the solid phase, red the liquid phase and dashed the melting temperature. For  $\beta = 100$  and  $R_0 = 10$  nm.

Finally, in Figure 6, we present temperature distributions throughout the melting process for the problem of Figure 3a. Plots for different conditions all take a similar form, so we only present this single result and in this case we show the dimensional values. The dashed line represents the temperature in the solid phase ( $0 < r < R(t)$ ), the solid line the temperature in the liquid phase ( $R(t) < r < R_0$ ), they meet on the dotted line which represents the melt temperature  $T_m(t)$ . The

final set of curves occur at  $t = 1.36\text{ps}$ . As  $R \rightarrow 0$  the speed of melting increases and so the melting should be complete shortly after this time. An interesting feature of this graph is that the temperature within the solid is greater than the melt temperature and this becomes more apparent as time increases. This presumably occurs because the melt temperature decreases faster than the solid can diffuse the temperature change at the boundary. So, unlike in standard Stefan problems, the temperature in the solid phase acts to speed up the melting. This high temperature was pointed out in [24] and attributed to superheating, where the solid is everywhere above the (variable) melt temperature. However other authors define superheating as a surface effect that refers to heating a solid above its bulk melting temperature [44, 37]. If we think of the melt temperature depression as representing the decrease in energy required for the solid particles to move to the liquid phase then it is clear that the bulk particles are not affected and so should not be described as superheated.

## 6. CONCLUSIONS

In this paper we have presented a mathematical model for the melting of a spherical nanoparticle. The initial system of two partial differential equations coupled to the Gibbs-Thomson relation for the melt temperature and a Stefan condition to determine the domain was reduced to the solution of two first order ordinary differential equations. The approximate solution showed excellent agreement with the numerical solution of the full system.

The beauty of the reduced system is that it makes clear which parameters control the melting process. In this case the dominant parameter turned out to be  $\Gamma = 2\sigma_{sl}T_m^*/R_0\rho_l L_m \Delta T$ . From this we see the obvious feature that changing the particle size or the temperature driving the melting has a controlling influence. The non-dimensional grouping also indicates that, for example, increasing surface tension by a given factor is equivalent to decreasing the initial radius by the same factor.

The one-phase formulation and the system with  $c_l = c_s$  was also examined, since these are standard simplifications. It was shown that for large values of  $\Gamma$  these formulations are inaccurate. However, as  $\Gamma$  decreased (from 6 to 0.6) the differences decreased and the simpler formulations proved sufficiently accurate.

An interesting feature of the two-phase solution is that the solid temperature is higher than the melt temperature. This is not a feature of standard melting problems and presumably occurs because the melt temperature decreases faster than diffusion occurs in the solid. So, in contrast to melting on the macroscale, on the nanoscale the solid acts to speed up the melting process. This feature, coupled to the melting point depression leads to the abrupt melting that is observed experimentally.

All analysis was based on continuum theory, which obviously breaks down for sufficiently small particles. The generalised Gibbs-Thomson relation was also

shown to break down, for gold this occurred around 1 nm. Hence all our results were cut off at this limit. For smaller particles, or to follow the melting process to its completion a non-continuum theory must be applied.

**Acknowledgements.** The research of TGM was supported by a Marie Curie International Reintegration Grant *Industrial applications of moving boundary problems* Grant no. FP7-256417 and Ministerio de Ciencia e Innovación Grant MTM2011-23789. FF acknowledges the support of a Centre de Recerca Matemàtica PhD grant.

## REFERENCES

- [1] P. Abragall and N-T Nguyen. *Nanofluidics*. Artech House, 1st edition, 2009.
- [2] F. Ahmad, A.K. Pandey, A.B. Herzog and J.B. Rose, C.P. Gerba, and S.A. Hashsham. Environmental applications and potential health implications of quantum dots. *J Nanopart Res*, 14(1038):doi:10.1007/s11051-012-1038-7, 2012.
- [3] V. Alexiades and A.D. Solomon. *Mathematical Modelling of Freezing and Melting Processes*. Hemisphere Publishing Corporation, 1st. edition, 1993.
- [4] P. Bergese, I. Colombo, D. Gervasoni, and L.E. Depero. Melting of nanostructured drugs embedded into a polymeric matrix. *J. Phys. Chem. B*, 108:15488–15493, 2004.
- [5] P. Buffat and J. P. Borel. Size effect on the melting temperature of gold particles. *Physical Review A*, 13(6):2287–2297, 1976.
- [6] T. Ben David, Y. Lereah, G. Deutsch, R. Kofman, and P. Cheyssac. Solid-liquid transition in ultra-fine lead particles. *Philosophical Magazine A*, 71(5):1135–1143, 1995.
- [7] S.H. Davis. *Theory of Solidification*. Cambridge University Press, 2001.
- [8] P.G. Debenedetti. *Metastable liquids, concepts and principles*. Princeton University Press, 1996.
- [9] J. D. Evans and J. R. King. Asymptotic results for the Stefan problem with kinetic undercooling. *Q.Jl Mech. App. Math.*, 53:449–473, 2000.
- [10] C. Faivre, D. Bellet, and G. Dolino. Phase transitions of fluids confined in porous silicon: A differential calorimetry investigation. *European Physical Journal B*, 7(1):19–36, 1999.
- [11] P. Ghosh, G. Han, M. De, C.K. Kim, and V.M. Rotello. Gold nanoparticles in delivery applications. *Adv. Drug Delivery Rev.*, 60:1307–1315, 2008.
- [12] A. O. Govorov, W. Zhang, T. Skeini, H. Richardson, J. Lee, and N. A. Kotov. Gold nanoparticle ensembles as heaters and actuators: melting and collective plasmon resonances. *Nanoscale Research Letters*, 1(1):84–90, 2006.
- [13] G. Guisbiers, M. Kazan, O. Van Overschelde, M. Wautelet, and S. Pereira. Mechanical and thermal properties of metallic and semiconductive nanostructures. *J. Phys. Chem. C*, 112:4097–4103, 2008.
- [14] O. Gulseren, F. Ercolessi, and E. Tosatti. Premelting of thin wires. *Physical Review B*, 51(11):7377–7380, 1995.
- [15] J. M. Hill. *One-Dimensional Stefan Problems: An Introduction*. Longman Scientific & Technical, 1st. edition, 1987.
- [16] E.J. Hinch. *Perturbation methods*. Cambridge University Press, 2000.
- [17] S. Karmakar, S. Kumar, R. Rinaldi, and G. Maruccio. Nano-electronics and spintronics with nanoparticles. *J. Phys.: Conf. Ser.*, 292(012002):doi:10.1088/1742-6596/292/1/012002, 2011.
- [18] R. Kofman, P. Cheyssac, Y. Lereah, and A. Stella. Melting of clusters approaching 0D. *The European Physical Journal D*, 9(1-4):441–444, 1999.

- [19] K. Koga, T. Ikeshoj, and K-I Sugawara. Size- and temperature-dependent structural transitions in gold nanoparticles. *Phys. Rev. Lett.*, 92(11):doi:10.1103/PhysRevLett.92.115507, 2004.
- [20] C.-L. Kuo and P. Clancy. Melting and freezing characteristics and structural properties of supported and unsupported gold nanoclusters. *J. Phys. Chem. B*, 109:13743–13754, 2005.
- [21] S. L. Lai, J. Y. Guo, V. Petrova, G. Ramanath, and L. H. Allen. Size-dependent melting properties of small tin particles: Nanocalorimetric measurements. *Physical Review Letters*, 77(1):99–102, 1996.
- [22] X. Liu, P. Yangb, and Q. Jiang. Size effect on melting temperature of nanostructured drugs. *Mat. Chem. Phys.* 103, 103:1–4, 2007.
- [23] S. W. McCue, J. R. King, and D. S. Riley. Extinction behaviour for two-dimensional inward-solidification problems. *Proc. R. Soc. A*, 459(2032):977–999, 2003.
- [24] S. W. McCue, B. Wu, and J. M. Hill. Micro/nanoparticle melting with spherical symmetry and surface tension. *IMA J. Appl. Math.*, 74:439–457, 2009.
- [25] S.L. Mitchell and M. Vynnycky. Finite-difference methods with increased accuracy and correct initialization for one-dimensional Stefan problems. *Applied Mathematics and Computation*, 215(4):1609–1621, 2009.
- [26] T. G. Myers, S. L. Mitchell, and F. Font. Energy conservation in the one-phase supercooled Stefan problem. *Int. Commun. Heat and Mass Transf.*, 2012.
- [27] K.K. Nanda. Size dependent melting of nanoparticles. *Pramana J. Phys.*, 72(4):617–628, 2009.
- [28] N-T Nguyen and S.T. Werely. *Fundamentals and applications of microfluidics*. Artech House, 1st edition, 2006.
- [29] O. Petrov and I. Furó. Curvature-dependent metastability of the solid phase and the freezing-melting hysteresis in pores. *Physical Review E*, 73:011608, 2006.
- [30] A. Plech, V. Kotaidis, S. Grésillon, C. Dahmen, and G. von Plessen. Laser-induced heating and melting of gold nanoparticles studied by time-resolved x-ray scattering. *Physical Review B*, 70(19):195423, 2004.
- [31] S. Rana, A. Bajaj, R. Mout, and V.M. Rotello. Monolayer coated gold nanoparticles for delivery applications. *Adv. Drug Delivery Rev.*, 64:200–216, 2012.
- [32] D. S. Riley, F. T. Smith, and G. Poots. The inward solidification of spheres and circular cylinders. *International Journal of Heat and Mass Transfer*, 17:1507–1516, 1974.
- [33] C. Ruan, Y. Murooka, R. K. Raman, and R. A. Murdick. Dynamics of size-selected gold nanoparticles studied by ultrafast electron nanocrystallography. *Nano Letters*, 7(5):1290–1296, 2007.
- [34] O.V. Salata. Applications of nanoparticles in biology and medicine. *J. Nanobiotech.*, 2(3), 2004.
- [35] V.M. Samsonov, A.N. Bazulev, and N.Yu. Sdobnyakovy. On applicability of Gibbs thermodynamics to nanoparticles. *Central European J. Phys.*, 1(3):474–484, 2003.
- [36] H. W. Sheng. Superheating and melting-point depression of Pb nanoparticles embedded in Al matrices. *Phil. Mag. Lett.*, 73(4):179–186, 1996.
- [37] H. W. Sheng, G. Ren, L. M. Peng, Z. Q. Hu, and K. Lu. Superheating and melting-point depression of Pb nanoparticles embedded in Al matrices. *Philosophical Magazine Letters*, 73(4):179–186, 1996.
- [38] J.-H. Shim, B.-J. Lee, and Y. W. Cho. Thermal stability of unsupported gold nanoparticle: a molecular dynamics study. *Surf. Sci.*, 512:262i<sub>2</sub><sup>1</sup>268, 2002.
- [39] K. P. Travis, B. D. Todd, and D. J. Evans. Departure from navier-stokes hydrodynamics in confined liquids. *Physical Review E*, 55(4):4288–4295, 1997.
- [40] S. Volz, J-B Saulnier, M. Lallemand, B. Perrin, and P. Depondt. Transient fourier-law deviation by molecular dynamics in solid argon. *Phys. Rev. B*, 54(1):340–347, 1996.



- [41] B. Wu, S. W. McCue, P. Tillman, and J. M. Hill. Single phase limit for melting nanoparticles. *Applied Mathematical Modelling*, 33(5):2349–2367, 2009.
- [42] B. Wu, P. Tillman, S. W. McCue, and J. M. Hill. Nanoparticle melting as a Stefan moving boundary problem. *Journal of Nanoscience and Nanotechnology*, 9(2):885–888, 2009.
- [43] T. Wu, H.-C. Liaw, and Y.-Z. Chen. Thermal effect of surface tension on the inward solidification of spheres. *International Journal of Heat and Mass Transfer*, 45(10):2055–2065, 2002.
- [44] J. Zhong, L. H. Zhang, Z. H. Jin, M. L. Sui, and K. Lu. Superheating of Ag nanoparticles embedded in Ni matrix. *Acta Materialia*, 49(15):2897–2904, 2001.

F. FONT

CENTRE DE RECERCA MATEMÀTICA  
CAMPUS DE BELLATERRA, EDIFICI C  
08193 BELLATERRA  
BARCELONA, SPAIN

AND

DEPARTAMENT DE MATEMÀTICA APLICADA I  
UNIVERSITAT POLITÈCNICA DE CATALUNYA  
BARCELONA, SPAIN

*E-mail address:* `ffont@crm.cat`

T.G. MYERS

CENTRE DE RECERCA MATEMÀTICA  
CAMPUS DE BELLATERRA, EDIFICI C  
08193 BELLATERRA  
BARCELONA, SPAIN

*E-mail address:* `tmyers@crm.cat`



